

Collectivism in a Replication Network of Minimal Nucleobase Sequences

Sonia Vela-Gallego

Universidad Autonoma de Madrid

Zulay Pardo-Botero

IMDEA Nanociencia <https://orcid.org/0000-0002-1472-4849>

Cristian Moya-Álamo

Universidad Autonoma de Madrid <https://orcid.org/0000-0001-5107-7751>

Andrés de la Escosura (✉ andres.delaescosura@uam.es)

Universidad Autónoma de Madrid <https://orcid.org/0000-0002-0928-8317>

Article

Keywords: replication, different, pathways, network, amino, cysteine, kinetic

Posted Date: November 3rd, 2021

DOI: <https://doi.org/10.21203/rs.3.rs-927381/v1>

License: © ⓘ This work is licensed under a Creative Commons Attribution 4.0 International License.

[Read Full License](#)

1 Collectivism in a Replication Network of Minimal Nucleobase Sequences

2 Sonia Vela-Gallego,^{*a} Zulay Pardo-Botero,^b Cristian Moya-Álamo,^a Andrés de la Escosura^{*a,c}

3 ^[a] *Department of Organic Chemistry, Universidad Autónoma de Madrid, Campus de Cantoblanco,*
4 *28049 Madrid, Spain.*

5 ^[b] *IMDEA Nanociencia, C/ Faraday 7, 28049 Madrid, Spain.*

6 ^[c] *Institute for Advanced Research in Chemistry (IAdChem), Cantoblanco, 28049 Madrid, Spain.*

7 * *Corresponding authors: S.V.G: sonia.vela@uam.es; A.d.l.E: andres.delaescosura@uam.es.*

8

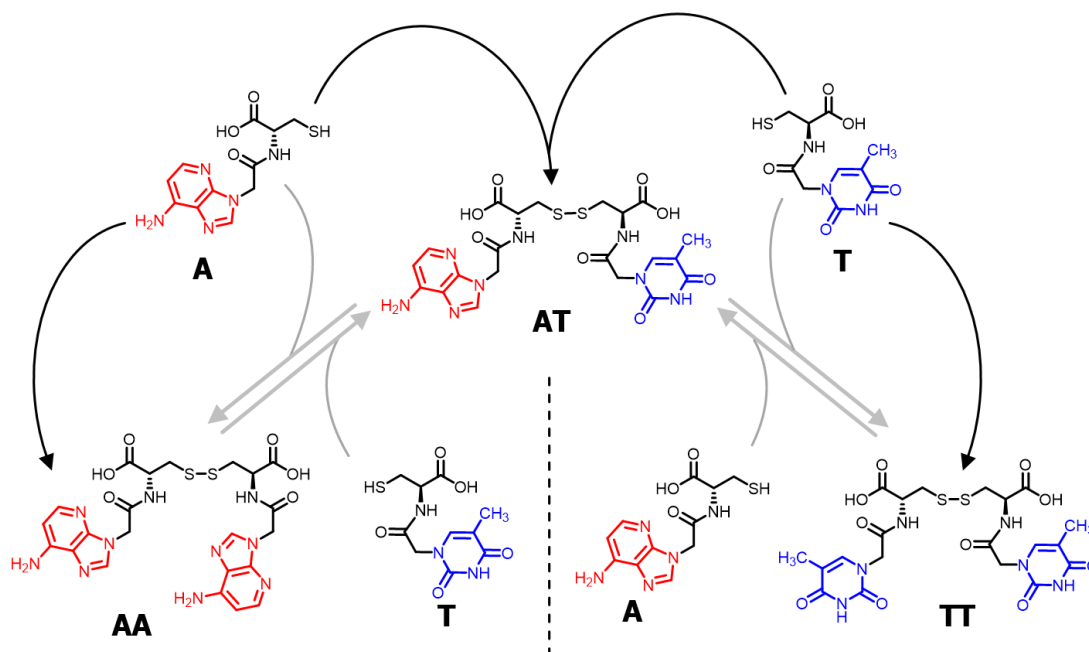
9 **Abstract.** A major challenge for understanding the origins of life is to explore how replication
10 networks can engage in an evolutionary process. Herein, we shed light on this problem by
11 implementing a network constituted by two different types of extremely simple biological
12 components: the amino acid cysteine and the canonical nucleobases adenine and thymine,
13 connected through amide bonds to the cysteine amino group and oxidation of its thiol into three
14 possible disulfides. Supramolecular and kinetic analyses revealed that both self- and mutual
15 interactions between such dinucleobase compounds drive their assembly and replication
16 pathways. Those pathways involving sequence complementarity led to enhanced replication
17 rates, suggesting a potential bias for selection. The interplay of synergistic dynamics and
18 competition between replicators was then simulated in an open reactor with experimental kinetic
19 data, showing the selective amplification of different species depending on the initial mixture
20 composition. Overall, this network configuration can favor a collective adaptability to changes
21 in the availability of feedstock molecules, with disulfide exchange reactions serving as 'wires'
22 that connect the different individual auto- and cross-catalytic pathways.

23 Research on life's origins constitutes a major multidisciplinary effort to unravel the
24 physicochemical means by which living systems could emerge from non-living matter. Many
25 questions remain open in the field, with implications that are both historical (how and where life
26 originated), synthetic (how life can be synthesized from its basic molecular constituents), and
27 conceptual (what essential features of living organisms allow characterization of their
28 aliveness).¹⁻⁵ Systems chemistry is proving to be useful in this respect, as it adopts a holistic
29 view for the study of complex chemical systems, wherein dynamic out-of-equilibrium reaction
30 and self-assembly processes govern the system's emergent behaviors.⁶⁻⁸ An important line in
31 this area involves the development of chimeric systems that combine the properties of distinct
32 biological building blocks, as a step towards replication, protometabolic networks and
33 protocellular assemblies.⁹⁻¹³

34 In the endeavor to mimic DNA's capacity for replication or, more generally, the capacity of
35 living cells to self-reproduce, different forms of replication have been developed with both
36 synthetic and biological molecules.¹⁴⁻¹⁸ The literature is rich in processes that display
37 *autocatalysis*, either through the product's catalysis of its own formation,¹⁹ *cyclic*
38 *autocatalysis*,^{20,21} or in oscillatory reactions.²² Most of these autocatalytic transformations
39 cannot be considered self-replication, since they lack the specificity required for information
40 transfer at the molecular level.¹⁸ In search for such specificity, *template replication* has been
41 proven with different kinds of biopolymers and oligomers, including DNA,^{23,24} RNA^{25,26} and
42 oligopeptides,^{27,28} as well as with synthetic molecules not present in extant biology.²⁹ However,
43 this type of mechanism tends to halt the replication process due to an excessively strong binding
44 (and therefore inhibition) of the template and product molecules, which handicaps efforts to
45 achieve exponential product growth. *Network autocatalysis* has been proposed as an
46 alternative,^{30,31} with both theoretical and experimental models based on lipids,^{32,33} peptides,^{34,35}
47 nucleic acids,³⁶ and synthetic molecules.³⁷ Autocatalysis in these networks is normally
48 associated with self-assembly of the replicating species, most commonly into hybridized
49 strands, fibers, micelles or vesicles, the latter being relevant to the formation of self-reproducing

50 compartments.^{32,38} This type of replication was likely widespread in prebiotic scenarios, but in
51 order to trigger subsequent evolution, replicators would have to acquire additional capacities
52 including:³⁹ (i) catalysis, to establish a supportive metabolism;⁴⁰ (ii) performance out of
53 equilibrium;^{35,41,42} (iii) compartmentalization, to avoid parasitic reactions and dilution effects;⁴³
54 or (iv) variability control with nucleobase sequences.⁴⁴ Important open questions with respect to
55 nucleobase sequences are how simple can be their constituent monomers, and what is the
56 minimal sequence length that can drive the emergence of replication networks.

57 To shed light on those issues, herein we describe a new family of very simple exponential
58 replicators emerging from monomers that display adenine or thymine (**A** and **T**), connected
59 through amide bonds to the amino groups of cysteine (Figure 1). The role of the amino acid in
60 these molecules is to link the nucleobases in a sequence, through oxidation of its reactive thiol
61 into dynamic disulfide bonds. Despite the short length of these nucleobase sequences,
62 supramolecular studies showed that they are able to control the self-assembly of the three
63 formed species (**AA**, **TT** and **AT**), thus determining their replication efficiency. In-depth kinetic
64 experiments and simulations were used to study how the resulting aggregates affect the
65 irreversible auto- and cross-catalytic oxidation pathways of **A** and **T**, and the concomitant
66 reversible disulfide exchange reactions. In spite of the low complexity of the studied replicators,
67 both in terms of the monomers structure (much simpler than that of ribonucleotides) and of the
68 sequence length (dimers), complementarity of nucleobases enhanced the replication rate for
69 both the auto- and cross-catalytic pathways (**AT** and **AA/TT**, respectively), suggesting an
70 adaptive potential that involves the interplay of different collective and competitive dynamic
71 interactions between them.



72

73 **Figure 1.** Set of building blocks and transformations that constitute the reaction network under
 74 study. **A** and **T** are thiol monomers with a single nucleobase, and therefore lack the potential to
 75 self-assemble. Black arrows represent the oxidation of **A** and **T** into the disulfide dimers **AA**, **TT**
 76 and **AT**, which can occur in a non-catalyzed manner or alternatively via autocatalysis provided
 77 that they are in sufficient concentration to form 'catalytic' aggregates. Grey arrows represent
 78 disulfide exchange reactions. **AA** and **TT** can also replicate through cross-catalysis based on
 79 the complementarity of their nucleobase sequences.

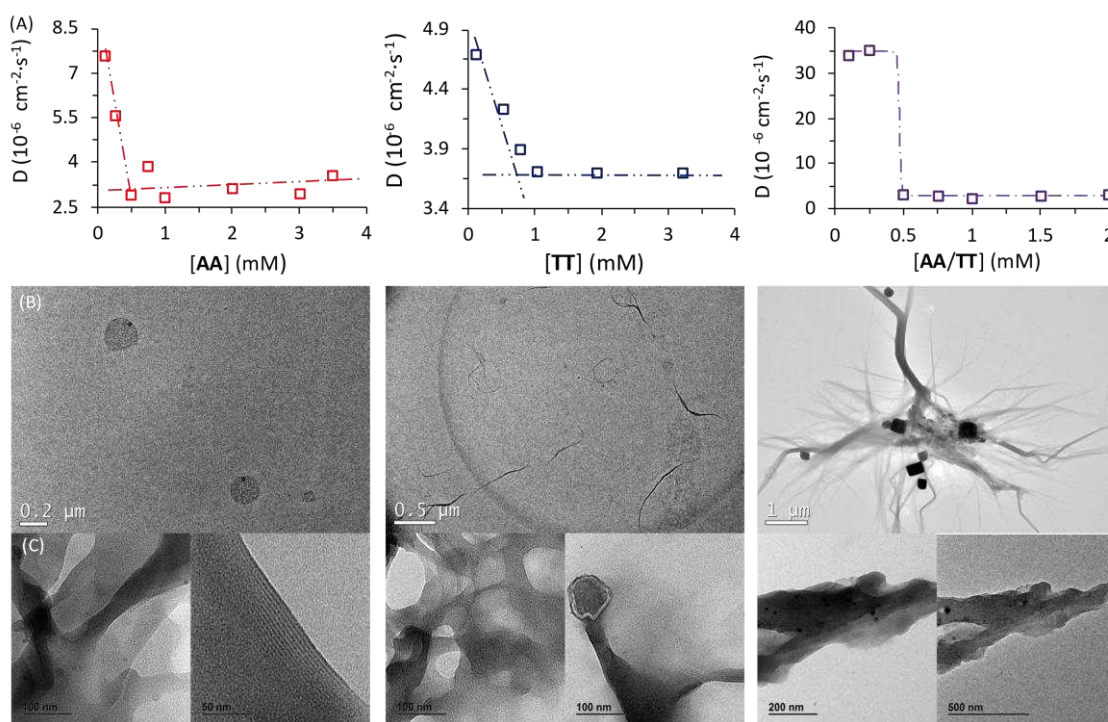
80

81 Results

82 **Synthesis and self-assembly of the network components.** The network building blocks (**A** and
 83 **T**) and the corresponding disulfide homodimers were synthesized and characterized as
 84 described in the supporting information (SI, Scheme S1). ¹H-NMR revealed a slow oxidation
 85 into disulfides in DMSO (Figure S1), completely stopped in acidic water (Figure S2 bottom),
 86 and fast in aqueous basic medium (pH 11; see Figure S2, top). One of the requisites to establish
 87 base pairing interactions between adenine and thymine, however, is that they stay non-ionized.

88 pH titrations, monitored by $^1\text{H-NMR}$, confirmed pK_a values of 4.14 ± 0.02 for the protonated
89 adenine moiety in **AA** (Figure S3A), and of 9.62 ± 0.03 for the dissociation of the thymine
90 imide NH in **TT** (Figure S3B). It can be assumed that similar pK_a values are applicable to **AT**,
91 which could not be separated from the homodimers when generated in a mixture of **A** and **T**.
92 On these bases, and considering that a slightly basic pH is optimum for disulfide
93 formation/exchange,³⁴ all the subsequent self-assembly and replication experiments were run in
94 50 mM borate buffer at pH 8.2.

95 The existence of aggregation under such conditions was demonstrated through diffusion-
96 ordered spectroscopy (DOSY) for samples containing **AA**, **TT** or an equimolar mixture of
97 **AA/TT** at different concentrations (from 0.1 to 4 mM). The diffusion coefficient (D) was
98 calculated for all samples, through monitoring of the monoexponential attenuation of NMR
99 signals during a pulsed field gradient experiment, followed by plotting the obtained D values
100 versus concentration (Figure 2A-C) to determine the critical aggregation concentration (cac).
101 Datasets with two clearly differentiated linear regions were obtained for **AA** and **TT**, with the
102 one above the cac showing a larger and constant D value, indicative of the presence of higher-
103 order aggregates. The intersection between the two lines pointed to specific cac values of 0.51
104 and 0.9 mM, respectively. For the **AA/TT** mixture, a different data distribution was obtained,
105 with a sharp transition between the aggregated and non-aggregated states. A cac value of 0.47
106 mM was obtained by fitting the data with a Boltzmann equation ($R^2 = 0.9993$) to detect the
107 slope changing point, suggesting that nucleobase sequence complementarity induces a stronger
108 and cooperative self-assembly.



109

110 **Figure 2.** Supramolecular studies of compounds **AA**, **TT**, and an equimolar mixture of **AA/TT**.
 111 (A) Plot of the diffusion coefficient (D) obtained by DOSY experiments versus the concentration
 112 of **AA** (left), **TT** (middle) and **AA/TT** (right). Critical aggregation concentration (cac) values
 113 were calculated as the intersection of two straight lines in the plots for **AA** and **TT**, and through
 114 fitting to a Boltzmann-type equation for **AA/TT**. (B, C) TEM micrographs of **AA** (left), **TT**
 115 (middle) and **AA/TT** (right) at two different concentrations: 1 mM (B) and 2 mM (C) in 50 mM
 116 borate buffer (pH 8.2).

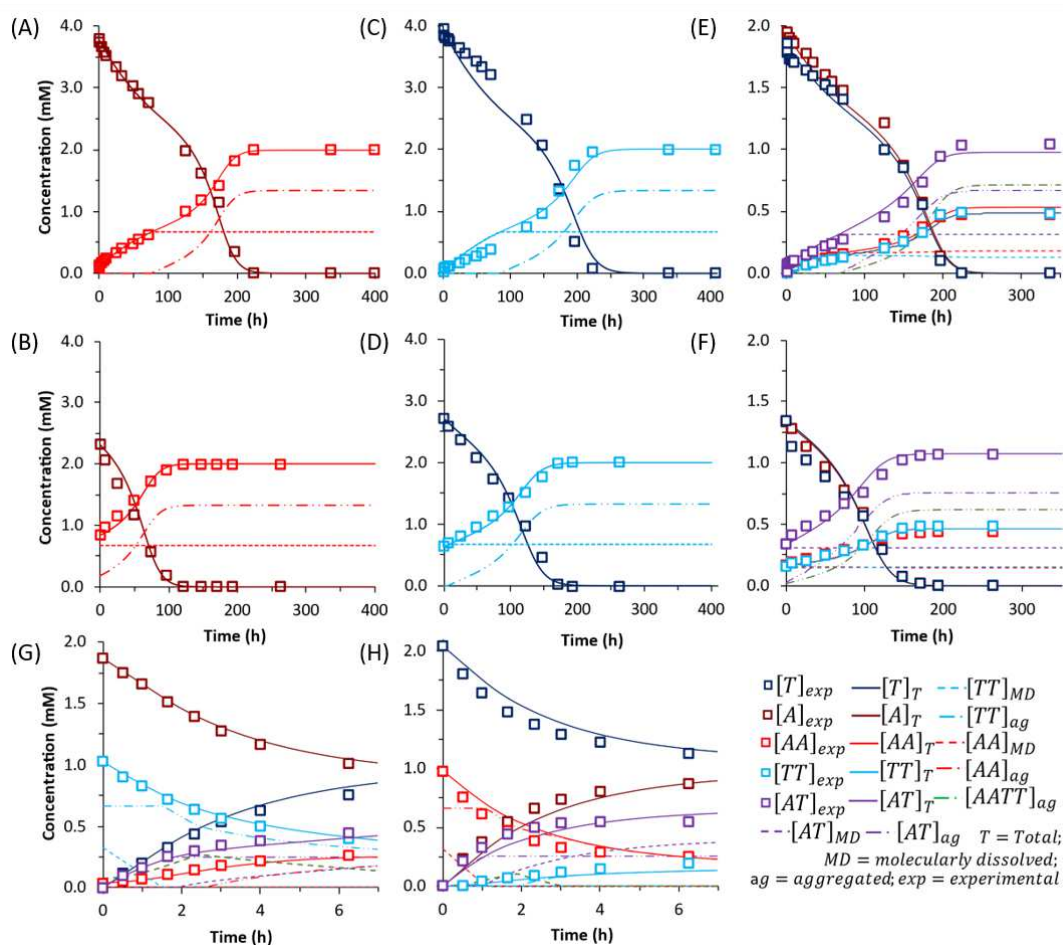
117 To assess the morphology of those aggregates, TEM studies were conducted at two different
 118 disulfide concentrations: 1 and 2 mM (Figure 2B and 2C, respectively). At 1 mM, the low
 119 density of objects over the grid indicated minor aggregation of **AA** and **TT**, showing spherical
 120 assemblies for the former (Figure 2B left / S5A), yet they were very exceptional and may not be
 121 representative of the main self-assembly pathway, and isolated fibrils for the latter (Figure 2B
 122 middle / S6A). Despite their low abundance, the presence of sulfur detected by energy
 123 dispersive x-ray spectroscopy (EDS) confirmed that such structures were formed by the
 124 corresponding disulfide compounds. For the **AA/TT** mixture, intertwined fiber assemblies were
 125 observed over the whole grid (Figure 2B right / S7A), in a significantly higher abundance than

126 for **AA** or **TT** alone. This points to the importance of complementary nucleobase pairing to
127 induce aggregation in the mixture. At the high concentration, aggregation was much more
128 prominent (Figure 2C) and resulted in lamellar structures for all cases, probably as a result of
129 the hierarchical assembly of fibers into sheets. The distance between adjacent sheets could be
130 clearly determined in areas where the lamellar arrangement was perpendicular with respect to
131 the grid surface, yielding similar values (~4 nm) for **AA** and **TT** (Figure S5B/S6B bottom). For
132 **AA/TT**, the stronger aggregation gave rise to thicker stacks of sheets (Figure 2B right / S7B)
133 that did not permit estimation of the interlamellar distance. In any case, the formation of
134 different assemblies for the three systems, including fibers and lamellar structures depending on
135 concentration, points to a complex assembly landscape, with contribution from hydrogen
136 bonding interactions, nucleobase π - π stacking and hydrophobic effects. The involved self-
137 assembly mechanisms will be examined in-depth in subsequent studies but, since previous work
138 has demonstrated the capacity of fibrillar and sheet assemblies to facilitate replication
139 processes,^{34,45} we assume these to be the catalytically active ones also in the present case.

140 **Replication experiments.** The initial replication experiments were performed with only one
141 monomer, either **A** or **T**, at 4 mM concentration. The reaction kinetics were monitored through
142 reverse phase high-performance liquid chromatography (HPLC, see experimental section and
143 Figures S8-S11), coupled to electrospray ionization mass spectrometry (ESI-MS) for
144 identification of species. For the non-templated oxidation reactions, Figures S8/S9 show a
145 gradual decay of monomer and growth of dimer elution peak areas over the course of the
146 experiment. Calibration curves were performed for **A**, **T**, **AA** and **TT** in order to quantify their
147 molar concentrations in each aliquot (Figures S12-S15). The kinetic profiles, plotted from the
148 obtained concentrations at different reaction times, showed typical features of autocatalysis for
149 both **AA** and **TT** (Figure 3A, B): an initial slow growth of product (induction period) followed
150 by a phase of faster growth (autocatalysis) until full conversion of monomer into dimer.
151 Importantly, the change in curve slope was observed at a product concentration that
152 approximately matches its *cac* value, as determined by DOSY, proving that there is no

153 autocatalysis in the absence of aggregates (below the *cac*). To confirm the products'
154 autocatalytic nature, seeded experiments with 30% of **AA** or **TT** were conducted, maintaining
155 the total concentration of starting materials in the same range as in the non-templated reactions.
156 In both cases, a shortening of the induction period and an overall decrease in the reaction time
157 was observed (Figure 3C, D; while Figure S16A and S16B shows the direct comparison of
158 seeded and non-seeded experiments), indicating that they actually contribute to increase the
159 reaction rate. This effect was less prominent for **TT**, probably due to its lower tendency to
160 aggregate (higher *cac*).

161 Similar results were obtained when conducting the reactions from a mixture of **A** and **T** (2
162 mM each). Figure 3E depicts the kinetic profiles obtained from HPLC monitoring over time
163 (Figure S10), revealing the characteristic features of replication kinetics for both **AA**, **TT** and
164 **AT**. Experiments seeded with 20% of a previously finished reaction resulted in a shortening of
165 the induction period for the three replicating species (Figure 3F, S16C and S16D). However, the
166 scenario becomes significantly more complex when the two nucleobases are present, as
167 disulfide exchange reactions can also occur. To study the role of these exchange processes in the
168 global network kinetics, two different reactions were performed (4 mM **T** + 2 mM **AA** and 4
169 mM **A** + 2 mM **TT**) with HPLC monitoring (Figure S11). In the obtained kinetic curves, two
170 stages could be distinguished, the first one corresponding to a preeminent role of disulfide
171 exchange during the first 7 h of the reaction (Figure 3G and 3H).



172

173 **Figure 3.** Kinetic profiles corresponding to: (first row) the autocatalytic formation of AA (A),
 174 TT (C), and the mixture of possible replicators AA/TT/AT (E); (second row) seeded
 175 experiments for the autocatalytic formation of AA (B), TT (D), and AA/TT/AT (F); (third row)
 176 disulfide exchange reactions (up to 7 h) between AA and T (G) or TT and A (H). Each panel
 177 shows the evolution of all involved species over time through experimental data (square data
 178 points) and fit curves, while the set of kinetic equations used for fitting are depicted in Table 1.
 179 In the templated reactions (A, C, E), the total concentration of starting materials was
 180 maintained in the same range as in the non-templated ones (B, D, F), with minor experimental
 181 deviations that are difficult to avoid but are considered in the mathematical analysis. The non-
 182 seeded experiments were repeated three times, while seeded experiments and disulfide exchange
 183 reactions were repeated twice (Figures S16-S19). The treatment of fitting errors with such
 184 repeats is shown in section 6 of the SI.

185 **Kinetic analyses.** The above replication data were used to analyze the contribution of all
186 involved processes in the global network kinetics. Two different reactions were initially
187 considered for the formation of each disulfide homodimer: the non-catalyzed (**R-A1**, **R-T1**) and
188 the autocatalytic oxidation (**R-A2**, **R-T2**) of the corresponding monomeric thiol (Table 1, boxes
189 1 and 2). In the reaction schemes, **AA_{ag}** and **TT_{ag}** refer to the self-assembled products, and
190 emerge from the aggregation processes **R-A3** and **R-T3**. For calculation of kinetic constants, the
191 concentration of aggregated replicator is needed at any given time. According to Chen *et al.*,⁴⁶
192 the concentrations of **AA_{ag}** and **TT_{ag}** are given by equation **Eq-S1** (Section 5 in the SI), in
193 which the total concentration of aggregating compound (C_T) can be expressed as a function of
194 C_I (the concentration of molecularly dissolved compound), ρ (a parameter related to the
195 reaction mechanism) and K_{eq} (the equilibrium constant of the aggregation process). This
196 equation can become complex to solve, but the problem is approachable considering that when
197 C_T is below $1/K_{eq}$, most molecules are in the monomeric form, whereas molecules aggregate
198 rapidly if C_T exceeds that value. An equivalence can therefore be assumed between $1/K_{eq}$ and
199 the *cac*, an assumption that is valid for any possible aggregation mechanism. In Figure S20, for
200 example, when the analytical solutions of **Eq-S1** for different values of ρ are compared to the
201 proposed simplification, the outcome differences are negligible.

202 The rate equations for non-catalyzed (**Eq-A1** and **Eq-T1**) and autocatalytic regimes (**Eq-A2**
203 and **Eq-T2**) were defined in a MATLAB program (Table 1, boxes 1 and 2), establishing that
204 they operate below and above the *cac*, respectively. For autocatalytic processes, the mechanism
205 of catalysis was not known and so equations with different orders with respect to both **A** (or **T**)
206 and **AA_{ag}** (or **TT_{ag}**) were evaluated through fitting of the experimental data. The equilibrium
207 constants of aggregate formation were considered through equations **Eq-A3** and **Eq-T3**. The
208 best fitting curves can be seen in Figures 3A-D (with R^2 above 0.99 in all cases), and
209 correspond to a global order of three for the autocatalytic stage (**Eq-A2** and **Eq-T2**) and two
210 with respect to the aggregated replicator. For a complete statistical treatment of fitting errors,
211 see section 6 of the SI, Tables S1-S3 and Figures S21 and S22. The fact that the best fittings

212 were obtained for a reaction order of two with respect to the replicating species (therefore
213 higher than one) points to an exponential growth.^{34,47} The orders obtained in the rate equations
214 **Eq-A2** and **Eq-T2** actually imply that in the 'catalytic' hybrid assemblies of monomeric thiol
215 and disulfide dimer, the required ratio between both for the monomer to get activated towards
216 oxidation is of 1:2. Further studies will however be devoted to propose a solid mechanistic
217 scheme of this replication process. In any case, it is worth mentioning that the kinetic constants
218 for the catalyzed reactions were about one order of magnitude greater than the non-catalyzed
219 ones. The calculated equilibrium constants ($K_{AA_{ag}} = 1.95 \text{ mM}^{-1}$ and $K_{TT_{ag}} = 1.6 \text{ mM}^{-1}$) in turn led
220 to *cac* values of 0.51 and 0.63 mM, respectively, which are close to those obtained from DOSY
221 experiments.

222 A similar procedure was applied for calculation of disulfide exchange kinetic constants,
223 considering four possible reactions/equations (**R-E1** to **R-E4** / **Eq-E1** to **Eq-E4** -- Table 1, box
224 3; fitting curves in Figure 3G, H) and all previously calculated constants (k_A , k_T , k_{Ac} , k_{Tc} , $K_{AA_{ag}}$
225 and $K_{TT_{ag}}$). The constants resulting upon fitting (k_{e1} , k_{e2} , k_{e3} , k_{e4}) are approximately one order of
226 magnitude larger than those for the autocatalytic oxidation of monomeric thiols, which makes
227 their reaction rates comparable. Concerning the analysis of replication from mixtures of both
228 nucleobase monomers, the landscape of non-covalent assembly pathways is more complex than
229 for single replicators. In addition to the self-assembly of **AA** and **TT**, two other aggregate types
230 must be considered, resulting from either complementary interaction between **AA** and **TT**
231 (**AATT_{ag}**) or from self-pairing of **AT** (i.e., **AT_{ag}**). These aggregates enable auto- and cross-
232 catalytic reactions, as **AATT_{ag}** can aid in reactions producing **AA** and **TT** (**R-A4** and **R-T4**,
233 respectively – Table 1, box 4), and **AT_{ag}** can assist in its own formation (**R-AT2**) (Table 1, box
234 5). For mathematical fitting of these processes (Figure 3E, F), all constants concerning the non-
235 catalyzed and autocatalytic formation of **TT** and **AA**, the disulfide exchange reactions, the
236 aggregation constants of **AA** and **TT** and the order of those reactions with respect to aggregates
237 in the autocatalytic regime were used as previously calculated.

238 **Table 1.** Kinetic analysis of the replication network. Boxes 1 and 2 concern the irreversible
239 reactions (either non-catalyzed or autocatalytic) of oxidation of **A** and **T** into **AA** and **TT**,
240 respectively, and the equilibrium of aggregation of the latter species, as the resulting
241 aggregates are involved in the autocatalysis. Box 3 includes the four possible disulfide
242 exchange reaction steps. Boxes 4 and 5 refer to the cross-catalysis of **AA/TT** and the
243 autocatalysis of **AT**, respectively. In all boxes, the table details each of the involved processes,
244 the equations that govern them and the values of the resulting rate/equilibrium constants. The
245 order of the reactions, with respect to the monomers and the catalytic aggregates, in equations
246 **Eq-A2**, **Eq-T2**, **Eq-A4**, **Eq-T4** and **Eq-AT2** was determined through fitting of the experimental
247 data into rate equations with different orders (see Tables S1-S3), selecting those that led to the
248 lowest mean absolute percentage errors and R^2 values > 0.99 . Dispersion graphs for the
249 different fits (Figures S21 and S22) helped confirming the selected rate equations.

	Reaction	Equation	Constant
Box 1	R-A1 $A + A \rightarrow AA$	Eq-A1 $k_A[A]^2$	$k_A = 6.62 \cdot 10^{-4} \text{ mM}^{-1} \text{ h}^{-1}$
	R-A2 $A + A \xrightarrow{AA_{ag}} AA$	Eq-A2 $k_{Ac}[A][AA_{ag}]^2$	$k_{Ac} = 1.38 \cdot 10^{-2} \text{ mM}^{-2} \text{ h}^{-1}$
	R-A3 $AA + AA \rightleftharpoons AA_{ag}$	Eq-A3 $K_{eqAAag} = 1/[AA]_{cac}$	$K_{eqAAag} = 1.95 \text{ mM}^{-1}$
Box 2	R-T1 $T + T \rightarrow TT$	Eq-T1 $k_T[T]^2$	$k_T = 6.89 \cdot 10^{-4} \text{ mM}^{-1} \text{ h}^{-1}$
	R-T2 $T + T \xrightarrow{TT_{ag}} TT$	Eq-T2 $k_{Tc}[T][TT_{ag}]^2$	$k_{Tc} = 1.73 \cdot 10^{-2} \text{ mM}^{-2} \text{ h}^{-1}$
	R-T3 $TT + TT \rightleftharpoons TT_{ag}$	Eq-T3 $K_{eqTTag} = 1/[TT]_{cac}$	$K_{eqTTag} = 1.6 \text{ mM}^{-1}$
Box 3	R-E1 $A + TT_d \xrightarrow{K_{e1}} T + AT_d$	Eq-E1 $k_{e1}[A][TT]_{MD}$	$k_{e1} = 0.15 \text{ mM}^{-1} \text{ h}^{-1}$
	R-E2 $T + AA_d \xrightarrow{K_{e2}} A + AT_d$	Eq-E2 $k_{e2}[T][AA]_{MD}$	$k_{e2} = 0.21 \text{ mM}^{-1} \text{ h}^{-1}$
	R-E3 $A + AT_d \xrightarrow{K_{e3}} T + AA_d$	Eq-E3 $k_{e3}[A][AT]_{MD}$	$k_{e3} = 0.11 \text{ mM}^{-1} \text{ h}^{-1}$
	R-E4 $T + AT_d \xrightarrow{K_{e4}} A + TT_d$	Eq-E4 $k_{e4}[T][AT]_{MD}$	$k_{e4} = 0.07 \text{ mM}^{-1} \text{ h}^{-1}$
Box 4	R-A4 $A + A \xrightarrow{AATT_{ag}} AA$	Eq-A4 $k_{AATT1}[A][AATT]_{ag}^2$	$k_{AATT} = 5.86 \cdot 10^{-2} \text{ mM}^{-2} \text{ h}^{-2}$
	R-T4 $T + T \xrightarrow{AATT_{ag}} TT$	Eq-T4 $k_{AATT2}[T][AATT]_{ag}^2$	$k_{AATTc} = 6.02 \cdot 10^{-2} \text{ mM}^{-2} \text{ h}^{-2}$
	R-AATT $AA + TT \rightleftharpoons AATT_{ag}$	Eq-AATT $K_{eqAATTag} = 1/[AATT]_{cac}$	$K_{eqAATTag} = 3.27 \text{ mM}^{-1}$
Box 5	R-AT1 $A + T \rightarrow AT$	Eq-AT1 $k_{AT}[A][T]$	$k_{AT} = 1.54 \cdot 10^{-3} \text{ mM}^{-1} \text{ h}^{-1}$
	R-AT2 $A + T \xrightarrow{AT_{ag}} AT$	Eq-AT2 $k_{ATc}[A]^{0.5}[T]^{0.5}[AT]_{ag}^2$	$k_{ATc} = 4.69 \cdot 10^{-2} \text{ mM}^{-2} \text{ h}^{-2}$
	R-AT3 $AT + AT \rightleftharpoons AT_{ag}$	Eq-AT3 $K_{eqATag} = 1/[AT]_{cac}$	$K_{eqATag} = 3.25 \text{ mM}^{-1}$

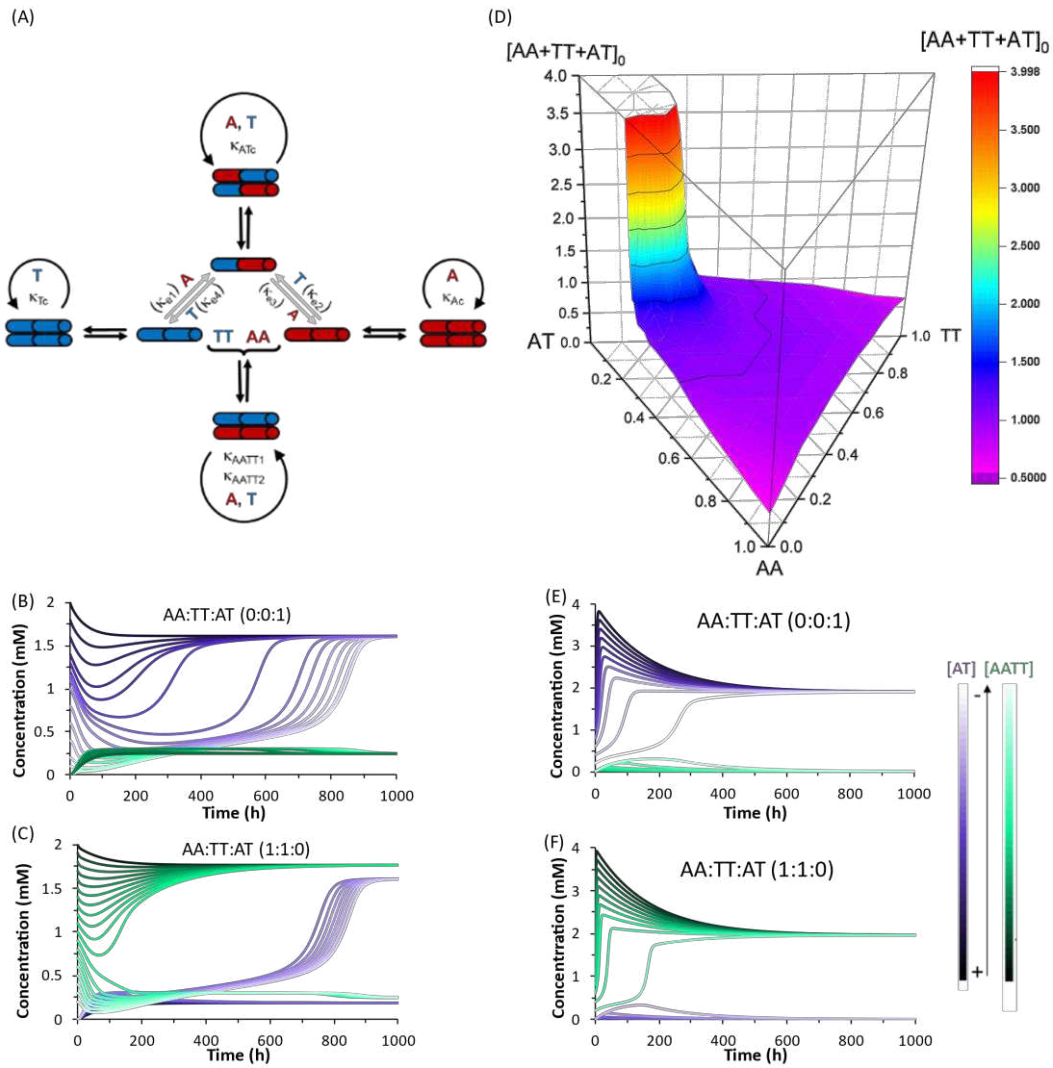
250

251 This global analysis of the network kinetics revealed interesting aspects of its behavior. As
252 expected, for statistical reasons related to the number of pathways to its formation, **AT** is
253 produced twice as fast as **AA** or **TT**. More importantly, the auto-/cross-catalytic reactions were
254 ~4x faster, and the aggregation constants 2x higher when there is complementarity between
255 nucleobase sequences (i.e. for **AT** and **AA/TT**) than when there is not (i.e., for **AA** or **TT**).
256 Indeed, according to the calculated K_{ag} values for both \mathbf{AATT}_{ag} and \mathbf{AT}_{ag} (3.3 mM^{-1}), their *cac*
257 would correspond to 0.3 mM (total concentration of disulfides), in agreement with the DOSY
258 data. These minimal nucleobase sequences therefore seem to enhance their replication through
259 complementary base pairing.

260 *Interplay between synergistic/self-replication pathways.* According to the above kinetic
261 analysis, the network topology presents two dominant competing pathways: the autocatalytic
262 replication of **AT** (Figure 4A, top cycle); and the synergistic assembly of **AA/TT**, which results
263 in cross-catalysis towards their common formation (Figure 4A, bottom cycle). In a closed
264 reactor, fast disulfide exchange contributes to balance both pathways, leading to a statistical
265 mixture of the three replicating species. In contrast, in an open reactor, the asymmetry between
266 both competing pathways, together with their possible interconversion through exchange
267 reactions, may lead to adaptive behaviors.⁴⁸ To predict the evolutionary potential of this network
268 topology in open environments, a continuous perfect mixing reactor (section 5 in the SI) was
269 modeled in excel software using the previously determined kinetic data. In the studied
270 configuration, the 20 mL reactor could be initially loaded with any possible combination of the
271 three species and continuously fed with monomers **A** and **T** (4 mM) through two different input
272 streams of 1 $\mu\text{L}/\text{min}$, while maintaining a constant reactor volume through the extraction of an
273 equivalent output current.

274 When starting from an empty reactor ($[\text{replicators}]_0 = 0$), the system evolved as expected into
275 a steady state dominated by **AT** (SS_{AT}), where $[\text{AT}] = 1.61 \text{ mM}$ and $[\text{AA/TT}] = 0.24 \text{ mM}$, the
276 latter meaning total disulfide concentration (Figure 4B, lightest color curves). A significant
277 decrease in the time needed to reach SS_{AT} was observed when loading the reactor with

278 increasing initial **AT** concentrations (Figure 4B). SS_{AT} was also obtained when the reactor was
279 filled with **AA/TT** below a threshold concentration (see below). When $[AA/TT]_0$ was above
280 that threshold, however, a new steady state appeared ($SS_{AA/TT}$) where **AA/TT** were the dominant
281 species ($[AA/TT] = 1.77$ mM) and **AT** decreased in concentration ($[AT] = 0.19$ mM) (Figure
282 4C and S23). A range of initial proportions of **AA**, **TT** and **AT**, and of total initial disulfide
283 concentration (from 0 to 4 mM), was then tested to determine which steady state would be
284 reached in each case. The result was a 3D surface (Figure 4D) that marks the boundary between
285 initial conditions that favor SS_{AT} (below the surface) or $SS_{AA/TT}$ (above the surface).
286 Interestingly, the threshold below which **AT** always gets amplified was ~ 1 mM; above that
287 threshold, $SS_{AA/TT}$ was favored except when the initial molar fraction of **AT** was higher than 0.8.
288



289

290 **Figure 4.** (A) Replication network topology. (B, C) Simulations of the network evolution when
 291 fed with two input streams ($Q_{in} = 1 \mu\text{L}/\text{min}$) of **A** and **T**, in the presence of replicator **AT** ($0 - 2$
 292 mM) (B) or **AA/TT** ($0 - 2 \text{ mM}$) (C). (D) 3D surface representing the reached steady state (SS_{AT}
 293 below the surface; $SS_{AA/TT}$ above) for a range of initial replicator proportions (horizontal axes
 294 on the graph) and total replicator concentrations (vertical axis). The surface marks the
 295 boundary between initial conditions that favor SS_{AT} (below the surface) or $SS_{AA/TT}$ (above). (E,
 296 F) Simulations of the network evolution when decreasing the exchange constants by six orders
 297 of magnitude, with the same input streams and conditions as in (B) and (C).

298 The capacity of a dynamic system to reach two different steady states depending on the
 299 initial conditions is called bistability, and in the present case it seems to be related to their
 300 possible interconversion through disulfide exchange. To test this possibility, the network

301 behavior was simulated in a hypothetical scenario where the exchange reactions were kinetically
302 frozen, artificially reducing the values of their kinetic constants by six orders of magnitude
303 compared to the experimental data (see Table S4). In that situation, the dominant species in the
304 reached steady state correlated exclusively with the replicating system (**AT** or **AA/TT**) initially
305 present (Figure 4E and 4F). In addition, the concentration of the ‘losing’ replicative system
306 drops almost to extinction. The reason for this is that, in the absence of exchange reactions, the
307 dominant catalytic species gets amplified sufficiently quickly to consume all the substrates fed
308 into the reactor. This simulation thus proves the importance of disulfide exchange as wiring
309 reactions that connect the different auto- and cross-catalytic pathways, endowing the whole
310 replication network with a collectively better adaptability, as it can switch from one replicating
311 system to the other if the conditions are favorable.

312

313 **Conclusions**

314 The results of this work underscore the likelihood of replication networks emerging in
315 conditions and from building blocks with reasonable prebiotic plausibility. The replicating
316 species are built from the amino acid cysteine and two canonical nucleobases, which have been
317 reported in Miller-type experiments,⁴⁹ Strecker-derived chemistry⁵⁰ and HCN/cyanoacetylene
318 oligomerization reactions.⁵¹ Although for practical reasons our synthesis of **A** and **T** was
319 performed following standard organic synthesis techniques, the chemistry of amide and
320 disulfide bond formation/exchange has been extensively studied in prebiotic contexts.² More
321 importantly, the molecular complexity of the replicators **AA**, **TT** and **AT** is significantly less
322 than that of other different replicator families reported to date, suggesting that the structural
323 requirements for chemical evolution to step into replicating species was probably not so high.
324 The present cysteine-based derivatives do not need an oligopeptide or lipid chain to drive their
325 self-assembly and replication processes. On the other hand, the smallest nucleic acid template
326 replicators previously described required a minimum sequence of 6 nucleotides.¹⁵ As a merge of
327 both approaches, the self-assembly of **AA**, **TT** and **AT** must be mostly promoted by H-bond

328 interactions between nucleobases, together with π - π stacking and hydrophobic effects. Despite
329 this makes their self-assembly weaker and the replication rates slower compared to previous
330 peptide- or lipid-based replicators, they gain a rudimentary sequence-based control of the
331 replication process. Building on such a capacity, the network described herein presents a
332 collective behaviour that can provide significant adaptability between the individual synergistic
333 and 'selfish' replication pathways, aided by exchange reactions that allow interconversion
334 between the different replicator species.

335

336 **Methods**

337 Complete procedures for the synthesis and characterization of the network components are
338 described in the SI.

339 *Self-assembly and replication experiments.* A borate-buffered solution (200 mM, pH 8.2) was
340 employed for all the self-assembly and replication experiments. Boric acid (20 mmol, 1.24 g)
341 was dissolved in H₂O (100 ml), or D₂O for the DOSY experiments, and the pH was adjusted to
342 8.2 with 1 M aq. NaOH (or NaOD). This buffer was used as a stock to prepare all samples,
343 adjusting the borate concentration to 50 mM in all cases.

344 *Transmission electron microscopy and energy dispersive x-ray spectroscopy* was performed in
345 a JEOL JEM-2100 electron microscope (JEOL Ltd., Tokyo, Japan) operated at 200 kV,
346 preparing samples as follows: 5 μ L of sample solution were applied to glow discharged
347 formvar/carbon-coated grids. Images were acquired with a CCD ORIUS SC1000 camera.

348 *DOSY NMR.* Different solutions of **AA**, **TT** or equimolar mixtures of **AA/TT** (0.1, 0.25, 0.5,
349 0.75, 1, 2, 3 and 4 mM total concentration of disulfide) were prepared in D₂O-based borate
350 buffer, and the pH was readjusted to 8.2. The DOSY measurements were performed using the
351 longitudinal eddy current (LED) delay pulse sequence. The duration of the magnetic field pulse
352 gradient (small delta, δ) was 2.8 ms and the diffusion delay (big delta, Δ) was 100 ms in order to
353 obtain less than 3% residual signal with the maximum gradient strength. The number of

354 accumulated scans (ns) was set between 32 and 80 depending of the sample concentration. The
355 pulse gradients were incremented in ns steps from 2% to 95% of the maximum gradient strength
356 (53.5 G/cm) in a linear ramp. The Eddy Current delay (t_e) and the pulse separation (t_s) were set
357 at 5 and 0.2 ms, respectively, in all experiments. For details on the calculation of D , see section
358 2 in the SI.

359 **Replication experiments.** A solution of **A** or **T** (5.3 mM) in water (for the one-component
360 autocatalytic reactions), or an equimolar mixture of **A** and **T** (2.7 mM each for the two-
361 component replication processes) was vortexed for 1 min, followed by addition of borate buffer
362 (200 mM) until dilution to 4 mM of monomer (total cysteine concentration) and 50 mM of
363 buffer. The mixture was vortexed for 1 min, and the pH was readjusted to 8.2 with NaOH (1
364 mM). The reaction was stirred at 600 rpm and 20 °C, and monitored through HPLC. Each
365 experiment was repeated at 3 times.

366 **Seeded replication experiments.** Monomer solutions, either with a single component or with an
367 equimolar mixture of **A** and **T**, were prepared as described in the previous paragraph. Once
368 prepared and while being stirred, the corresponding percentage of seed (20/30% of cysteine)
369 from a finished reaction was added, and the reaction was kept stirring at 600 rpm and 20 °C,
370 followed by HPLC monitoring. Each experiment was repeated twice.

371 **Disulfide exchange reactions.** A solution of **A** (4 mM) in borate buffer (50 mM) was prepared
372 as described above, and mixed with a finalized oxidation reaction of **T** (containing 100 mol% of
373 **TT**) in a 2:1 molar ratio of **A/TT**. The protocol for the opposite reaction (**T + AA**) was identical
374 except for the switch of the nucleobases in the monomeric thiol and the disulfide derivative. The
375 reaction was stirred at 600 rpm and 20 °C, and monitored through HPLC, repeating twice each
376 of the experiments.

377 **HPLC-MS.** 50 μ L aliquots from every experiment were collected at the indicated times and
378 deposited into 1% aqueous TFA to quench the reaction. The samples were then frozen until
379 analyzed in a Waters Symmetry® C18 5 μ m 250 \times 4.6 mm column, eluting them with a linear

380 gradient of water to acetonitrile for 15 min. The different species were identified with a single
381 quadrupole mass detector and quantified with a UV-Vis detector ($\lambda = 260$ nm).

382 **Acknowledgements**

383 This research was supported by the H2020 FET-Open (A.d.l.E and G.A.; CLASSY project,
384 Grant Agreement N° 862081) and the Spanish Ministry of Economy and Competitiveness (A.d.l.E;
385 MINECO: CTQ-2014-53673-P, CTQ-2017-89539-P, and EUIN2017-87022). We would like to
386 acknowledge Dr. Ana Pizarro for her advice in the NMR determination of the nucleobase pK_a
387 values in compounds **AA** and **TT**, and Dr. Francisco Tato for initial tests on HPLC separations.
388 The professional editing service NB Revisions was used for technical preparation of the text
389 prior to submission.

390 **Author contributions**

391 S.V.G performed the experiments, Z.P.B. contributed to the DOSY analyses, C.M.A.
392 contributed to the computational kinetic analyses, A.d.l.E. conceived the project, S.V.G. and
393 A.d.l.E. contributed to designing and analyzing the experiments, and writing and editing the
394 manuscript.

395 **Competing interests**

396 The authors declare no competing interests.

397

398 **References**

-
1. Cronin, L. & Walker, S. I. Beyond prebiotic chemistry. *Science* **352**, 1174–1175 (2016).
 2. Ruiz-Mirazo, K., Briones, C. & de la Escosura, A. Prebiotic systems chemistry: new perspectives for the origins of life. *Chem. Rev.* **114**, 285–366 (2014).
 3. Szostak, J. W. The narrow road to the deep past: in search of the chemistry of the origin of life. *Angew. Chem. Int. Ed.* **56**, 11037–11043 (2017).

-
4. Sutherland, J. D. Studies on the origin of life—the end of the beginning. *Nat. Rev. Chem.* **1**, 1–7 (2017).
 5. Krishnamurthy, R. & Hud, N. V. Introduction: chemical evolution and the origins of life. *Chem. Rev.* **120**, 4613–4615 (2020).
 6. Ashkenasy, G., Hermans, T. M., Otto, S. & Taylor, A. F. Systems chemistry. *Chem. Soc. Rev.* **46**, 2543–2554 (2017).
 7. Ura, Y., Beierle, J. M., Leman, L. J., L. E. Orgel, M. R. Ghadiri. Self-assembling sequence-adaptive peptide nucleic acids. *Science* **325**, 73–77 (2009).
 8. Carbajo, D., Pérez, Y., Bujons, J. & Alfonso, I. Live-cell-templated dynamic combinatorial chemistry. *Angew. Chem.* **132**, 17355–17359 (2020).
 9. Mann, S. Systems of creation: the emergence of life from nonliving matter. *Acc. Chem. Res.* **45**, 2131–2141 (2012).
 10. Gibard, C., Bhowmik, S., Karki, M., Kim, E. K., & Krishnamurthy, R. Phosphorylation, oligomerization and self-assembly in water under potential prebiotic conditions. *Nat. Chem.* **10**, 212 (2018).
 11. Bonfio, C., Godino, E., Corsini, M., de Biani, F. F., Guella, G. & Mansy, S. S. Prebiotic iron–sulfur peptide catalysts generate a pH gradient across model membranes of late protocells. *Nat. Catal.* **1**, 616–623 (2018).
 12. Morales-Reina, S., Giri, C., Leclercq, M., Vela-Gallego, S., de la Torre, I., Castón, J. R., Surin, M. & de la Escosura, A. Programmed recognition between complementary dinucleolipids to control the self-assembly of lipidic amphiphiles. *Chem. Eur. J.* **26**, 1082–1090 (2020).
 13. Frenkel-Pinter, M., Haynes, J. W., Mohyeldin, A. M., Martin, C., Sargon, A. B., Petrov, A. S., Krishnamurthy, R., Hud, N. V., Williams, L. D. & Leman, L. J. Mutually stabilizing interactions between proto-peptides and RNA. *Nat. Commun.* **11**, 1–14 (2020).
 14. Paul, N. & Joyce, G. F. Minimal self-replicating systems. *Curr. Opin. Chem. Biol.* **8**, 634–639 (2004).
 15. Patzke, V. & von Kiedrowski, G. Self-replicating systems. *Arkivoc* **5**, 293–310 (2007).

-
16. Bissette, A. J. & Fletcher, S. P. Mechanisms of autocatalysis. *Angew. Chem. Int. Ed.* **52**, 12800–12826 (2013).
 17. Kosikova, T. & Philp, D. Exploring the emergence of complexity using synthetic replicators. *Chem. Soc. Rev.* **46**, 7274–7305 (2017).
 18. Adamski, P., Eleveld, M., Sood, A., Kun, Á., Szilágyi, A., Czárán, T., Szathmáry, E. & Otto, S. From self-replication to replicator systems en route to de novo life. *Nat. Rev. Chem.* **4**, 386–403 (2020).
 19. Soai, K., Shibata, T., Morioka, H. & Choji, K. Asymmetric autocatalysis and amplification of enantiomeric excess of a chiral molecule. *Nature* **378**, 767–768 (1995).
 20. Breslow, R. On the mechanism of the formose reaction. *Tetrahedron Lett.* **1**, 22–26 (1959).
 21. Hein, J. E. & Blackmond, D. G. On the origin of single chirality of amino acids and sugars in biogenesis. *Acc. Chem. Res.* **45**, 2045–2054 (2012).
 22. Epstein, I. R. & Showalter, K. Nonlinear chemical dynamics: oscillations, patterns, and chaos. *J. Phys. Chem.* **100**, 13132–13147 (1996).
 23. von Kiedrowski, G. A self-replicating hexadeoxynucleotide. *Angew. Chem. Int. Ed.* **25**, 932–935 (1986).
 24. Kreysing, M., Keil, L., Lanzmich, S. & Braun, D. Heat flux across an open pore enables the continuous replication and selection of oligonucleotides towards increasing length. *Nat. Chem.* **7**, 203–208 (2015).
 25. Hayden, E. J. & Lehman, N. Self-assembly of a group I intron from inactive oligonucleotide fragments. *Chem. Biol.* **13**, 909–918 (2006).
 26. Lincoln, T. A. & Joyce, G. F. Self-sustained replication of an RNA enzyme. *Science* **323**, 1229–1232 (2009).
 27. Lee, D. H., Granja, J. R., Martinez, J. A., Severin, K. & Ghadiri, M. R. A self-replicating peptide. *Nature* **382**, 525–528 (1996).
 28. Mukherjee, R., Cohen-Luria, R., Wagner, N. & Ashkenasy, G. A bistable switch in dynamic thiodepsipeptide folding and template-directed ligation. *Angew. Chem.* **127**, 12629–12633 (2015).

-
29. Tjivikua, T., Ballester, P. & Rebek Jr, J. A self-replicating system. *J. Am. Chem. Soc.* **112**, 1249–1250 (1990).
30. Kauffman, S. A. Autocatalytic sets of proteins. *J. Theor. Biol.* **119**, 1–24 (1986).
31. Vasas, V., Fernando, C., Santos, M., Kauffman, S., & Szathmáry, E. Evolution before genes. *Biol. Direct*, **7**, 1–14 (2012).
32. Segré, D., Ben-Eli, D., Deamer, D. W. & Lancet, D. The lipid world. *Orig. Life Evol. Biosph.* **31**, 119–145 (2001).
33. Colomer, I., Borissov, A. & Fletcher, S. P. Selection from a pool of self-assembling lipid replicators. *Nat. Commun.* **11**, 1–9 (2020).
34. Colomb-Delsuc, M., Sadownik, J. W., Mattia, E. & Otto, S. Exponential self-replication enabled through a fibre elongation/breakage mechanism. *Nat. Commun.* **6**, 7427 (2015).
35. Maity, I., Wagner, N., Mukherjee, R., Dev, D., Peacock-Lopez, E., Cohen-Luria, R. & Ashkenasy, G. A chemically fueled non-enzymatic bistable network. *Nat. Commun.* **10**, 1–9 (2019).
36. Arsène, S., Ameta, S., Lehman, N., Griffiths, A. D. & Nghe, P. Coupled catabolism and anabolism in autocatalytic RNA sets. *Nucleic Acids Res.* **46**, 9660–9666 (2018).
37. Semenov, S. N., Kraft, L. J., Ainla, A., Zhao, M., Baghbanzadeh, M., Campbell, V. E., Kang, K., Fox, J. M. & Whitesides, G. M. Autocatalytic, bistable, oscillatory networks of biologically relevant organic reactions. *Nature* **537**, 656–660 (2016).
38. Walde, P., Wick, R., Fresta, M., Mangone, A. & Luisi, P. L. Autopoietic self-reproduction of fatty acid vesicles. *J. Am. Chem. Soc.* **116**, 11649–11654 (1994).
39. Ruiz-Mirazo, K., Briones, C. & de la Escosura, A. Chemical roots of biological evolution: the origins of life as a process of development of autonomous functional systems. *Open Biol.* **7** 170050 (2017).
40. Santiago, G. M., Liu, K., Browne, W. R. & Otto, S. Emergence of light-driven protometabolism on recruitment of a photocatalytic cofactor by a self-replicator. *Nat. Chem.* **12**, 603–607 (2020).

-
41. Yang, S., Schaeffer, G., Mattia, E., Markovitch, O., Liu, K., Hussain, A. S., Ottel , J., Sood, A. & Otto, S. Chemical fueling enables molecular complexification of self-replicators. *Angew. Chem. Int. Ed.* **60**, 11344–11349 (2021).
42. Miao, X., Paikar, A., Lerner, B., Diskin-Posner, Y., Shmul, G., Semenov, S. N. Kinetic selection in the out-of-equilibrium autocatalytic reaction networks that produce macrocyclic peptides. *Angew. Chem. Int. Ed.* (2021). doi.org/10.1002/anie.202105790
43. Matsumura, S., Kun,  ., Ryckelynck, M., Coldren, F., Szil gyi, A., Jossinet, F., Rick, C., Nghe, P., Szathm ry, E. & Griffiths, A. D. Transient compartmentalization of RNA replicators prevents extinction due to parasites. *Science* **354**, 1293–1296 (2016).
44. Bandela, A. K., Wagner, N., Sadihov, H., Morales-Reina, S., Chotera-Ouda, A., Basu, K., Cohen-Luria, R., de la Escosura, A. & Ashkenasy, G. Primitive selection of the fittest emerging through functional synergy in nucleopeptide networks. *Proc. Natl. Acad. Sci. U.S.A.* **118**, e2015285118 (2021).
45. Rubinov, B., Wagner, N., Matmor, M., Regev, O., Ashkenasy, N. & Ashkenasy, G. Transient fibril structures facilitating non-enzymatic self-replication. *ACS Nano* **6**, 7893–7901 (2012).
46. Chen, Z., Lohr, A., Saha-M ller, C. R. & W rthner, F. Self-assembled π -stacks of functional dyes in solution: structural and thermodynamic features. *Chem. Soc. Rev.* **38**, 564–584 (2009).
47. von Kiedrowski, G. Minimal replicator theory I: parabolic versus exponential growth. *Bioorg. Chem. Front.* **3**, 113-146 (1993).
48. Wagner, N. & Ashkenasy, G. Rhythm before life. *Nat. Chem.* **11**, 681–683 (2019).
49. Parker, E. T., Cleaves, H. J., Dworkin, J. P., Glavin, D. P., Callahan, M., Aubrey, A., Lazcano, A. & Bada, J. L. Primordial synthesis of amines and amino acids in a 1958 Miller H₂S-rich spark discharge experiment. *Proc. Natl. Acad. Sci. U.S.A.* **108**, 5526–5531 (2011).
50. Foden, C. S., Islam, S., Fernandez-Garcia, C., Maugeri, L., Sheppard, T. D. & Powner, M. W. Prebiotic synthesis of cysteine peptides that catalyze peptide ligation in neutral water. *Science* **370**, 865–869 (2020).

-
51. Islam, S. & Powner, M. W. Prebiotic systems chemistry: complexity overcoming clutter. *Chem* **2**, 470–501 (2017).

Supplementary Files

This is a list of supplementary files associated with this preprint. Click to download.

- [VelaetalSICommunChem281021.pdf](#)